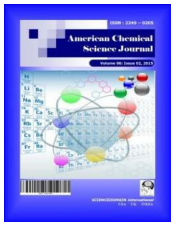

American Chemical Science Journal
16(3): 1-11, 2016, Article no.ACSJ.28258
ISSN: 2249-0205

SCIENCEDOMAIN *international*
www.sciencedomain.org

Thermal Properties, Crystal Structure, and Phase Transition of Racemic $CaC_4H_4O_6 \cdot 4H_2O$ Single Crystals

T. Fukami[1*], S. Hiyajyo[1], S. Tahara[1] and C. Yasuda[1]

[1]Department of Physics and Earth Sciences, Faculty of Science, University of the Ryukyus, Okinawa 903-0213, Japan.

Authors' contributions

This work was carried out in collaboration between all authors. Author TF performed measurements, managed the literature searches and wrote the first draft of the manuscript. Single crystals used were grown by author SH. Authors SH, ST and CY revised the manuscript and participated in group discussions. All authors read and approved the final manuscript.

Article Information

DOI: 10.9734/ACSJ/2016/28258
Editor(s):
(1) Mohammad Luqman, Department of Basic Science, College of Applied Sciences, A'Sharqiyah University, Oman.
(2) Nagatoshi Nishiwaki, Kochi University of Technology, Japan.
Reviewers:
(1) Anonymous, Georgia Southern University, USA.
(2) P. Selvarajan, Aditanar College of Arts and Science, Tiruchendur,Tamilnadu, India.
Complete Peer review History: http://www.sciencedomain.org/review-history/16006

Original Research Article

Received 12th July 2016
Accepted 25th August 2016
Published 1st September 2016

ABSTRACT

Single crystals of racemic calcium tartrate tetrahydrate, $CaC_4H_4O_6 \cdot 4H_2O$, were grown at 308 K by a gel method using silica gel as the medium of growth. Differential scanning calorimetry, thermogravimetric-differential thermal analysis, and X-ray diffraction measurements were performed on the single crystals. The space group symmetry (triclinic, $P\bar{1}$) and structural parameters were determined at room temperature. The O–H–O hydrogen-bonding networks formed between adjacent $C_4H_4O_6$ molecules, and between $C_4H_4O_6$ and H_2O molecules, were found to extend along the *c*-axis and $[0\bar{1}1]$ directions, respectively. A phase transition, driven by intramolecular proton transfer between three possible positions in the vicinity of O atoms, was found to occur at around 310 K. Weight losses due to thermal decomposition of racemic $CaC_4H_4O_6 \cdot 4H_2O$ occurred in the temperature range of 300–1200 K. The weight losses during decomposition were suggested to be caused by the evaporation of bound water molecules and the evolution of $2H_2CO$, $(1/2)O_2$, and 2CO gases.

**Corresponding author: E-mail: fukami@sci.u-ryukyu.ac.jp;*

Keywords: Racemic $CaC_4H_4O_6•4H_2O$; phase transition; proton transfer; thermal decomposition; DSC; TG-DTA; X-ray diffraction.

1. INTRODUCTION

Tartaric acid (chemical formula: $C_4H_6O_6$; systematic name: 2,3-dihydroxybutanedioic acid) is found in grapes, currants, gooseberries, oranges, apples, and in most acidulous fruits. It has two chiral carbon atoms in its molecule, which provides for four possible different forms of chiral, racemic, and achiral isomers: L(+)-tartaric, D(–)-tartaric, racemic (DL-) tartaric, and meso-tartaric acid [1–8]. The most common form in nature is L-tartaric acid; meso-tartaric acid is human-made and does not occur in nature. Solutions of L- and D-tartaric acid rotate the plane of polarized light to the left and to the right, respectively, whereas of DL- and meso-tartaric acid show no rotation of plane-polarized light. The optical properties of molecules derived from tartaric acid were discovered by Biot [9].

Many tartrate compounds are formed by the reaction of tartaric acid with compounds containing positive ions (two monovalent cations or one divalent cation). These compounds are used in numerous industrial applications, for example, as transducers and in linear and non-linear mechanical devices due to their excellent dielectric, ferroelectric, piezoelectric, and nonlinear optical properties [10–14]. Several types of tartaric acid crystals, such as potassium hydrogen tartrate ($KHC_4H_4O_6$), and calcium tartrate ($CaC_4H_4O_6$), develop naturally in bottled wine and are the major component of the harmless sediment found in wine [7,15–17]. The crystalline tartrate sediment as a by-product has to be removed from the wine after yeast fermentation of the grape juice. Louis Pasteur first separated the two enantiomers of sodium ammonium tartrate by utilizing the asymmetric habit of their crystals. In addition, he discovered the change in optical rotation induced by the different structures of each enantiomer in water solution [18–21]. The discovery of enantiomers has played an important role in advancing the scientific understanding of molecular chirality.

Recently, it has been found that single crystals obtained from kidney stones (renal calculi) in rats are composed of racemic (DL-) calcium tartrate tetrahydrate, $CaC_4H_4O_6·4H_2O$, as determined by powder and single crystal X-ray diffraction [22]. The crystal structure is triclinic with space group $P\bar{1}$. However, the reported structure may not be completely accurate based on the high *R*-value of the structure refinement (6.5% for 1495 independent reflections). Calcium ions required for the growth of kidney stones were included in the diet of rats (based on the AIN-93 formulation), but DL-tartaric acid was not present in the diet. Thus, it is presumed that potassium citrate monohydrate, $K_3C_6H_5O_7·H_2O$, included in the diet was converted to L- and D-tartaric acid in vivo, and the growth of kidney stones was induced by the calcium ions in the diet and the produced acids. Hence, the poor quality of the crystals suggests that the amounts of L- and D-tartaric acid were not sufficient for the growth of kidney stones, and rat kidney tissue may not be a suitable medium for crystal growth. We consider that the low-quality of single crystals obtained from kidney stones is most probably caused by the conditions of crystal growth. Silica gel is the most suitable medium to grow crystals with low solubility in water. Thus, high-quality single crystals of DL-$CaC_4H_4O_6·4H_2O$ would be grown by single diffusion method in silica gel medium containing DL-tartaric acid.

The purpose of this paper is to study the growth of single crystals of DL-$CaC_4H_4O_6·4H_2O$ using the gel method and to determine the exact crystal structure, including the positions of all hydrogen atoms, at room temperature using X-ray diffraction measurements. Moreover, the thermal properties of the DL-calcium salt are studied by means of differential scanning calorimetry (DSC) and thermogravimetric-differential thermal analysis (TG-DTA).

2. EXPERIMENTAL

2.1 Crystal Growth

Single crystals of $CaC_4H_4O_6$ were grown in silica gel medium at 308 K using the single test tube diffusion method. The gels were prepared in test tubes (length of 200 mm and diameter of 30 mm) using aqueous solutions of Na_2SiO_3 (22.4 g of 10.9 wt%), DL-$C_4H_6O_6$ (28.8 g of 13.0 wt%), and CH_3COOH (28.8 g of 13.0 wt%), and aged for several days. A solution of $CaCl_2$ (22.4 g of 7.4 wt%) was then gently poured on top of the gel. Many small crystals were grown at the gel matrix-solution interface, and the crystals (in size about $3×1×[5×10^{-1}]$mm) were harvested after one month. A typical photograph of six crystals grown by the gel method is shown in Fig. 1.

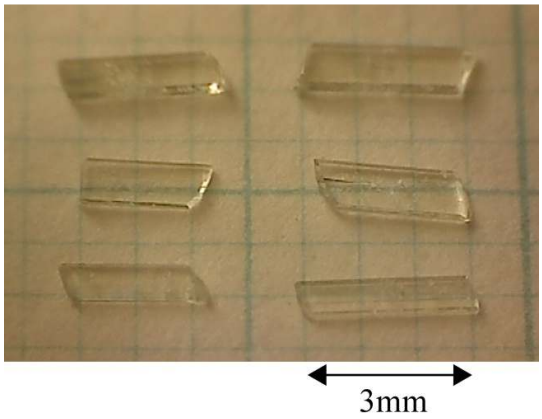

Fig. 1. Photograph of DL-$CaC_4H_4O_6 \cdot 4H_2O$ crystals grown by the gel method

2.2 Structure Determination

The X-ray diffraction measurements were carried out using a Rigaku Saturn CCD X-ray diffractometer with graphite-monochromated Mo K_α radiation (λ = 0.71073 Å). The diffraction data were collected at 298 K using an ω scan mode with a crystal-to-detector distance of 40 mm, and processed using the CrystalClear software package. The intensity data were corrected for Lorentz polarization and absorption effects. The structure was solved by direct methods using the SIR2011 program and refined on F^2 by full-matrix least-squares methods using the SHELXL-2013 program in the WinGX package [23–25].

2.3 Thermal Measurements

DSC and TG-DTA measurements were respectively carried out in the temperature ranges of 100–490 K and 300–1250 K, using DSC7020 and TG-DTA7300 systems from Seiko Instruments Inc. Aluminium (for DSC) and platinum (for TG-DTA) open pans with no pan cover were used as the measuring vessels and reference pans. Fine powder samples prepared by grinding many single crystals were used for the measurements. The sample amount varied between 3.41 and 4.78 mg, and the heating rates were either 5 or 10 K min^{-1} under the flow of nitrogen gas.

3. RESULTS AND DISCUSSION

3.1 Crystal Structure

The crystal structure of $CaC_4H_4O_6$ was determined by the single-crystal X-ray diffraction method at room temperature. The lattice parameters and intensity statistics obtained from all observed reflections reveal that the crystal belongs to triclinic system and centrosymmetric point group. Thus, the space group of $CaC_4H_4O_6$ was determined to be triclinic $P\bar{1}$ with cell parameters a = 6.2441(4) Å, b = 8.2208(5) Å, c = 10.4245(7) Å, α = 94.918(1)º, β = 105.947(2)º, and γ = 107.528(2)º. The atomic coordinates and thermal parameters for $CaC_4H_4O_6$, including the positions of all hydrogen atoms, were determined at room temperature. A final R-factor of 3.34% was calculated for 4202 unique observed reflections. The single crystals grown by the gel method presented in this study were found to be of racemic (DL-) calcium tartrate tetrahydrate, DL-$CaC_4H_4O_6 \cdot 4H_2O$. The relevant crystal data, and a summary of the intensity data collection and structure refinement parameters are given in Table 1. Fig. 2 shows a projected view of the DL-$CaC_4H_4O_6 \cdot 4H_2O$ crystal structure along the a-axis. The positional parameters in fractions of the unit cell, and the thermal parameters are listed in Table 2. Selected bond lengths (in Å) and angles (in degrees) are given in Table 3. The hydrogen-bond geometry (in Å and degrees) is presented in Table 4.

The observed lattice parameters are very similar to those of the single crystals obtained from rat kidney stones [22]. The obtained structure of the DL-calcium salt contains four crystallographically distinct water molecules, and is very similar to that observed in the crystals of kidney stones [22]. The fundamental features of the obtained structure are as follows. Each Ca atom in the unit cell is surrounded by eight O atoms at distances from 2.4011(7) to 2.5261(7) Å, forming a CaO_8 dodecahedron, as listed in Table 3. The average Ca–O distance is 2.450 Å. The lengths of six O–C bonds in the $C_4H_4O_6$ molecule are in the range of 1.254(1)–1.418(1) Å, as listed in Table 3. The variation in O–C distances is probably related to differences in bond type. The lengths of single and double O–C bonds in organic molecules are around 1.43 and 1.22 Å, respectively. The O(3)–C(2) and O(4)–C(3) bond lengths (hydroxyl group) are about 1.41 Å. Thus, these two O–C bonds have single bond character. Because the lengths of the remaining four O–C bonds are about 1.26 Å, these bonds have double bond character. Moreover, the lengths of three C–C bonds are in the range of 1.525(1)–1.544(1) Å. Because single C–C bonds in organic molecules are around 1.54 Å, the three bonds have single bond character. In the $C_4H_4O_6$ molecule, there is 180º rotational symmetry about the b-axis (which is perpendicular to the C(2)–C(3) bond). In fact,

Table 1. Crystal data, intensity collection and structure refinement parameters for DL-$CaC_4H_4O_6{\cdot}4H_2O$

Compound, M_r	$CaO_{10}C_4H_{12}$, 260.21
Crystal shape, color	Prism, colorless
Measurement temperature	298 K
Crystal system, space group	Triclinic, $P\bar{1}$
Lattice constants	a = 6.2441(4) Å, b = 8.2208(5) Å c = 10.4245(7) Å, α = 94.918(1)º β = 105.947(2)º, γ = 107.528(2)º
V, Z	482.27(5) $Å^3$, 2
D(cal.), μ(Mo K_α), F(000)	1.792 Mg m^{-3}, 0.692 mm^{-1}, 272
Crystal size	0.20 × 0.20 × 0.25 mm
θ range for data collection	2.07–38.07º
Index ranges	$-10 \le h \le 10$, $-14 \le k \le 13$, $-17 \le l \le 17$
Reflections collected, unique	13957, 4972 [R(int) = 0.0273]
Completeness to θ_{max}	94.5 %
Absorption correction type	Multi-scan
Transmission factor T_{min}–T_{max}	0.9077–1.0000
Date, parameter	4202 [$I>2\sigma(I)$], 185
Final R indices	R_1 = 0.0334, wR_2 = 0.0810
R indices (all data)	R_1 = 0.0432, wR_2 = 0.0872
Weighting scheme	$w = 1/[\sigma^2(F_o^2) + (0.0440P)^2]$ $P = (F_o^2 + 2F_c^2)/3$
Goodness-of-fit on F^2	1.071
Extinction coefficient	0.010(4)
Largest diff. peak and hole	0.403 and -0.410 e$Å^{-3}$

the O(1)–C(1), O(2)–C(1), and O(3)–C(2) bond lengths, and the O(1)–C(1)–O(2) and O(3)–C(2)–C(1) angles are almost the same as the O(6)–C(4), O(5)–C(4), and O(4)–C(3) bond lengths, and the O(6)–C(4)–O(5) and O(4)–C(3)–C(4) angles, respectively, as shown in Table 3. The angle between the two least-squares planes of atoms, O(1)O(2)O(3)C(1)C(2) and O(4)O(5)O(6)C(3)C(4), in the $C_4H_4O_6$ molecule is 44.76(3)º. The angles in the strontium tartaric, DL-tartaric acid, L- and D-tartaric acid crystals are 88.7(1), 72.79(4), 56.33(5), and 56.34(5)º, respectively [8,14]. Thus, the torsional strain in the $C_4H_4O_6$ molecule of the DL-calcium salt is smaller than that in these crystals.

There is a hydrogen-bonding network along the c-axis, connected by two O–H–O hydrogen bonds (O(3)–H(1)···O(5) and O(4)–H(2)···O(2)) between adjacent $C_4H_4O_6$ molecules, as shown in Fig. 2. The four H_2O molecules in the observed structure are located interstitially between two neighboring $C_4H_4O_6$ molecules, and form nine O–H–O hydrogen bonds with $C_4H_4O_6$ or H_2O molecules. There is also a hydrogen-bonding network along the [0 $\bar{1}$ 1] direction, consisting of the $C_4H_4O_6$ and H_2O molecules and the nine bonds, as shown in Fig. 2. The lengths of these nine bonds are in the range of 2.731(1)–3.205(1) Å, as listed in Table 4. The O(9)–H(10)–O(5) and O(9)–H(10)–O(6) hydrogen bonds are different from the other bonds because the H atom in these bonds is bound to the two O atoms. Three and four of the hydrogen bonds are shorter than the corresponding hydrogen bonds in the previously determined structures of $CaC_4H_4O_6{\cdot}4H_2O$ and $SrC_4H_4O_6{\cdot}4H_2O$, respectively [14–16]. The hydrogen bond strength is reflected by the bond length and the magnitude of electric charge at both ends of the bond. Because both O atoms at the ends have the same charge distribution, the strength of the hydrogen bond is determined by the bond length. Therefore, the averaged bonding strength in the DL-$CaC_4H_4O_6{\cdot}4H_2O$ crystal is stronger than that in the $CaC_4H_4O_6{\cdot}4H_2O$ and $SrC_4H_4O_6{\cdot}4H_2O$ crystals. Consequently, it is expected that the evaporation loss of hydrogen-bonded water molecules in the DL-calcium salt would occur at a higher temperature than that in these crystals.

3.2 Thermal Analysis

Fig. 3 shows the DSC curve of the DL-$CaC_4H_4O_6{\cdot}4H_2O$ crystal on heating in the temperature range from 100 to 490 K. The sample weight (powder) used for the measurement was 4.16 mg, and the heating rate was 5 K min^{-1} under a nitrogen gas flow of 40 ml min^{-1}. The sample used was one of three groups separated from the fine powder prepared by grinding single crystals. Small and large

endothermic peaks are clearly seen in the DSC curve at 312.2 and 387.8 K, respectively. The transition enthalpies ΔH (entropies ΔS) associated with these peaks were determined to be 2.73 (1.05R) and 136.6 kJ mol^{-1} (42.37R), respectively, where R is the gas constant (8.314 $JK^{-1}mol^{-1}$). No obvious endothermic or exothermic peaks were observed in the DSC curve between 100 and 312.2 K. In the measurements of the remaining samples, the peak temperatures (388.3 and 389.5 K) of the large endothermic peak observed were close to the first observed one of 387.8 K. However, the small endothermic peak was respectively observed at 306.5 and 321.2 K with ΔS of 1.02R and 1.18R, with a difference in peak temperature of ~15 K.

In general, it is believed that a clear peak in a DSC curve is attributed to the change of exchange energy at phase transition. Thus, the obtained results indicate that the phase transitions of DL-$CaC_4H_4O_6 \cdot 4H_2O$ occur at around 310 and 388 K, and there is no phase transition in the temperature range of 100–310 K. The peak temperature of 387.8 K is very close to the boiling point of water (373 K). Thus, it is expected that the peak at 387.8 K is attributed to the loss of water molecules from the sample due to evaporation. The observed temperature is higher than the evaporation temperature (355.7 K) of bound water in the $SrC_4H_4O_6 \cdot 4H_2O$ crystal, as previously reported [14]. As mentioned above, the difference in the evaporation temperature between the DL-calcium and strontium salts may be caused by the difference in bonding strength of the O–H–O hydrogen bonds formed by the four H_2O molecules.

The onset of the DSC peak at 387.8 K and the weight loss in the TG curve (as shown in Fig. 5 and described below) reveal that the evaporation loss of water begins at room temperature. The experimental conditions for all DSC measurements were identical, including the quality of the samples. Thus, the difference of ~15 K in temperature of the DSC peak around 310 K is considered to be caused by a difference in the amount of water contained in the three samples. Table 5 shows the peak temperatures, and transition enthalpies ΔH and entropies ΔS determined from the DSC curve.

Table 2. Atomic coordinates and thermal parameters (×10^4 Å^2) with standard deviations in brackets. The anisotropic thermal parameters are defined as exp[$-2\pi^2(U_{11}a^{*2}h^2 + U_{22}b^{*2}k^2 + U_{33}c^{*2}l^2 + 2U_{23}b^*c^*kl + 2U_{13}a^*c^*hl + 2U_{12}a^*b^*hk)$]. The isotropic thermal parameters (Å^2) for H atoms are listed under U_{11}

Atom	X	Y	z	U_{11}	U_{22}	U_{33}	U_{23}	U_{13}	U_{12}
Ca	0.34093(3)	0.18993(2)	0.27355(2)	168.6(9)	195.6(8)	169.7(8)	31.4(5)	35.3(6)	54.9(6)
C(1)	0.6173(2)	0.1512(1)	0.88742(8)	144(3)	216(3)	161(3)	33(3)	32(3)	48(3)
C(2)	0.4182(1)	0.1321(1)	0.75733(8)	156(3)	185(3)	152(3)	39(2)	26(2)	57(3)
C(3)	0.1917(1)	0.1287(1)	0.79172(8)	157(3)	187(3)	146(3)	28(2)	26(2)	61(3)
C(4)	0.0156(2)	0.1498(1)	0.66570(8)	181(4)	226(3)	171(3)	54(3)	48(3)	100(3)
O(1)	0.7021(1)	0.29609(9)	0.96546(7)	242(3)	220(3)	228(3)	-14(2)	-7(2)	43(2)
O(2)	0.6834(1)	0.02286(9)	0.90759(6)	260(3)	273(3)	173(3)	31(2)	6(2)	142(3)
O(3)	0.3788(1)	-0.02125(9)	0.66753(6)	249(3)	281(3)	138(2)	6(2)	18(2)	136(3)
O(4)	0.0881(1)	-0.02721(9)	0.83274(7)	175(3)	268(3)	169(3)	93(2)	20(2)	37(2)
O(5)	-0.1730(1)	0.0260(1)	0.60709(7)	187(3)	327(3)	214(3)	101(3)	-10(2)	33(3)
O(6)	0.0740(1)	0.29246(9)	0.62683(7)	326(4)	219(3)	266(3)	92(2)	46(3)	108(3)
O(7)	0.1405(1)	0.3448(1)	0.38339(8)	253(4)	309(3)	231(3)	39(3)	52(3)	118(3)
O(8)	0.1884(2)	0.3533(1)	0.10255(9)	249(4)	340(4)	387(4)	166(3)	23(3)	79(3)
O(9)	0.6013(2)	0.3120(1)	0.50375(8)	276(4)	308(4)	260(3)	-20(3)	-28(3)	129(3)
O(10)	0.6891(1)	0.3770(1)	0.22922(8)	297(4)	269(3)	267(3)	29(3)	92(3)	10(3)
H(1)	0.327(3)	-0.015(2)	0.587(2)	0.041(4)					
H(2)	0.155(3)	-0.027(2)	0.912(2)	0.043(4)					
H(3)	0.463(2)	0.226(1)	0.716(1)	0.013(3)					
H(4)	0.236(2)	0.230(2)	0.863(1)	0.023(3)					
H(5)	0.120(3)	0.321(2)	0.456(2)	0.050(5)					
H(6)	0.013(3)	0.335(2)	0.331(2)	0.062(5)					
H(7)	0.249(3)	0.451(2)	0.099(2)	0.046(4)					
H(8)	0.048(3)	0.329(2)	0.066(2)	0.041(4)					
H(9)	0.667(3)	0.420(2)	0.538(2)	0.051(5)					
H(10)	0.703(4)	0.273(3)	0.527(2)	0.089(7)					
H(11)	0.753(3)	0.478(2)	0.260(2)	0.042(4)					
H(12)	0.694(3)	0.369(2)	0.150(2)	0.049(5)					

Table 3. Selected interatomic distances (in Å) and angles (in degrees)

Ca–O(2)$^{(1)}$	2.4011(7)	Ca–O(3)$^{(1)}$	2.5261(7)
Ca–O(4)$^{(2)}$	2.4800(7)	Ca–C(4)$^{(2)}$	3.2388(9)
Ca–O(5)$^{(2)}$	2.4028(7)	Ca–O(7)	2.4488(8)
Ca–O(8)	2.4770(8)	Ca–O(9)	2.4227(8)
Ca–O(10)	2.4423(8)	O(1)–C(1)	1.257(1)
O(2)–C(1)	1.257(1)	O(3)–C(2)	1.418(1)
O(4)–C(3)	1.411(1)	O(5)–C(4)	1.254(1)
O(6)–C(4)	1.256(1)	C(1)–C(2)	1.526(1)
C(2)–C(3)	1.544(1)	C(3)–C(4)	1.525(1)
Ca$^{(1)}$–O(2)–C(1)	122.88(5)	Ca$^{(1)}$–O(3)–C(2)	119.26(5)
Ca$^{(2)}$–O(4)–C(3)	119.53(5)	Ca$^{(2)}$–O(5)–C(4)	121.46(5)
Ca$^{(2)}$–C(4)–O(5)	39.26(4)	Ca$^{(2)}$–C(4)–O(6)	156.23(6)
Ca$^{(2)}$–C(4)–C(3)	82.87(5)	O(1)–C(1)–O(2)	125.54(8)
O(1)–C(1)–C(2)	116.39(7)	O(2)–C(1)–C(2)	118.06(7)
O(3)–C(2)–C(1)	109.41(7)	O(3)–C(2)–C(3)	111.27(7)
O(4)–C(3)–C(2)	112.19(7)	O(4)–C(3)–C(4)	109.50(7)
O(5)–C(4)–O(6)	124.48(8)	O(5)–C(4)–C(3)	119.12(7)
O(6)–C(4)–C(3)	116.39(8)	C(1)–C(2)–C(3)	109.75(7)
C(4)–C(3)–C(2)	108.15(7)		

(Symmetry codes: (1) –x+1,–y,–z+1; (2) –x,–y,–z+1.)

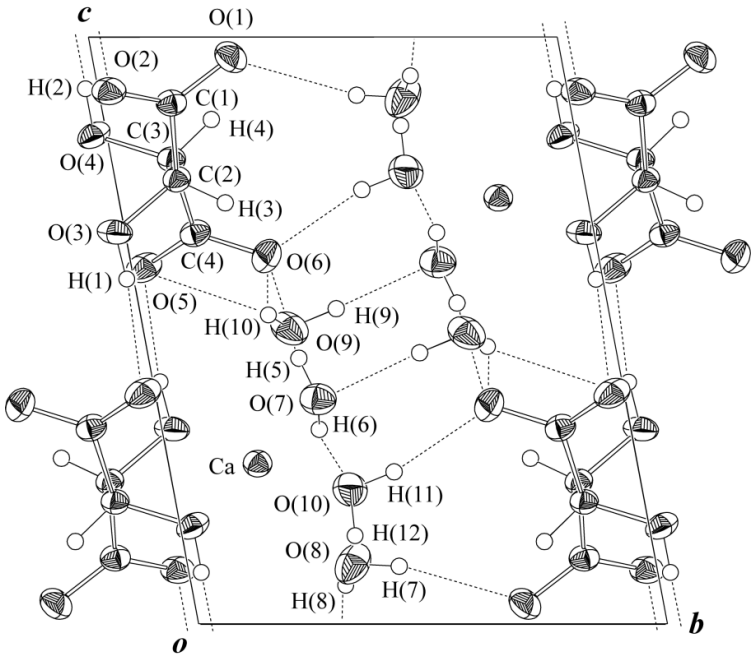

Fig. 2. ORTEP projection along the *a*-axis of DL-$CaC_4H_4O_6 \cdot 4H_2O$ structure with 60% probability-displacement thermal ellipsoids. The solid and short dashed lines show O–H···O hydrogen bonds shown in Table 4

The values of ΔS for the small peak observed in the DSC curves were in the range of 1.02*R*–1.18*R*, which is very close to *R* ln 3 (1.10*R*). This means that the number of steady states varies from one to three. We found two anomalous residual electron density peaks in the vicinity of the O(2) and O(3) atoms in the difference Fourier map taken after the final refinement cycle. Fig. 4 shows the difference electron density Fourier map in the vicinity of the O(2) and O(3) atoms along the *a*-axis, containing Fourier peaks corresponding to the O(2), O(3), C(1), and C(2) atoms and a difference Fourier peak corresponding to the H(1) atom. One of the two largest peaks in the difference Fourier map had an electron density of 0.23 eÅ^{-3} and was located

0.94 Å from the O(2) atom. The other large peak had a density of 0.20 eÅ^{-3} and was located 1.02 Å from the O(3) atom. The separation between the two residual density peaks was 1.13 Å. Moreover, the angle between the O(3)–H(1) bond and the position of the density peak (0.20 eÅ^{-3}) was 137º. From these results shown in Fig. 4, we deduced the nature of the phase transition occurring at around 310 K as follows. The H(1) atom bonded to the O(3) atom is located at the stable position at room temperature, as listed in Table 2. When above the transition temperature, the H(1) atom is transferred to the position of the density peak (0.20 eÅ^{-3}) by a 137º rotation about the O(3) atom. In addition, the atom prefers to move to the position of the density peak (0.23 eÅ^{-3}) and bonds to the O(2) atom. That is, the H(1) atom has the three possible positions in the vicinity of the O atoms shown in Fig. 4, and can be transferred between the three positions. The change of the number of steady states from one to three is produced by the transfer of the H(1) atom.

Fig. 5 shows the DTA, TG, and differential TG (DTG) curves of the DL-$CaC_4H_4O_6{\cdot}4H_2O$ crystal in the temperature range of 300–1250 K. The sample weight (powder) used for the measurement was 4.18 mg, and the heating rate was 10 K min^{-1} under a nitrogen gas flow of 300 ml min^{-1}. The DTA curve exhibits six endothermic peaks at 392.3, 556.0, 575.9, 749.1, 767.1, and 968.2 K. Peaks at 390.5, 562.6, 575.6, 724.7, 747.7, and 964.4 K, including a shoulder peak and very small peaks, are observed in the DTG curve. These DTG peaks almost correspond to the respective DTA peaks, except for the small peaks. The DTG curve, which is the first derivative of the TG curve, reveals the temperature dependence of the rate of weight loss. Thus, the DTA peaks are associated with the maximum rate of weight loss in the TG curve with increasing temperature. Table 5 shows the peak temperatures obtained from the DTA and DTG curves. Neither the peak nor the inflection (weight loss), corresponding to the small endothermic peak at around 310 K in the DSC curve, were not observed in the DTA, TG, or DTG curves. The small peak at around 310 K is very close to the start temperature on the TG-DTA measurement (room temperature), and the onset temperature of the large DTA peak at 392.3 K is also estimated to be around room temperature. Thus, no detection of a peak around 310 K in the DTA curve is probably due to its being obscured by decreasing the baseline of the curve at the start of measurement, and by the onset of the large peak. The lack of weight loss at around 310 K suggests that evaporation and evolution of gases do not occur at the transition temperature, and is consistent with the mechanism of proton transfer between the three possible positions described above.

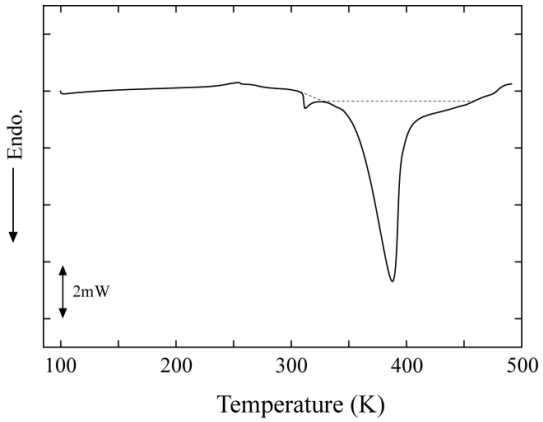

Fig. 3. DSC curve of DL-$CaC_4H_4O_6{\cdot}4H_2O$ crystal on heating. Sample weight (powder) was 4.16 mg and the heating rate was 5 K min^{-1} under N_2 gas flow of 40 ml min^{-1}

The TG curve shows the temperature dependence of the weight loss for the DL-$CaC_4H_4O_6{\cdot}4H_2O$ crystal. The weight loss around 390 K in the TG curve was determined to be 27.0% in the temperature range from 300 to 500 K. As mentioned above, we believe that the large endothermic peak at 392.3 K is caused by the evaporation of bound water molecules. The theoretical weight loss caused by the elimination of four H_2O molecules from the DL-$CaC_4H_4O_6{\cdot}4H_2O$ crystal is calculated to be 27.7% [=4×18.02/260.21]. This value is very close to the experimental weight loss of 27.0% around 390 K. Two small endothermic peaks, and the notable shoulder and large peaks at around 570 K were observed in the DTA and DTG curves, respectively. Generally, it is believed that the exothermic and endothermic heat peaks in DTA curve, accompanied by decomposition at high temperature, are due to the formation and loss of gas, respectively. Although no large exothermic peak was found at around 570 K, it seems that there is a very broad exothermic peak at a wide temperature range of 500–600 K. The two processes are considered to take place around this temperature, as is observed in the $SrC_4H_4O_6{\cdot}4H_2O$ crystal. We assume that the weight loss at 570 K is caused by the elimination of two moles of H_2CO gas, formed from $4H^+$ and $2CO^{2-}$ ions due to thermal decomposition. The

theoretical weight loss is calculated to be 23.1% [=2×30.03/260.21]. This value is close to the experimental weight loss of 20.8% observed at around 570 K, as determined from the TG curve in the temperature range from 500 to 660 K. Because small exothermic and endothermic peaks at around 750 K were found in the DTA curve, we believe that the formation of a half molar quantity of O_2 gas forms from the decomposition of CaC_2O_4, and the elimination of the gas occurs at around 750 K. The theoretical weight loss caused by the elimination of half a mole of O_2 gas is calculated to be 6.1% [=16.00/260.21]. This value is close to the experimental weight loss of 8.2% determined from the TG curve in the temperature range of 660–850K. Only one endothermic peak was observed at 968.2 K in the DTA curve, indicating that an evaporation reaction due to thermal decomposition occurs around the temperature. The theoretical weight loss caused by the evolution of two moles of CO gas is calculated to be 21.5% [=2×28.01/260.21]. This value is very close to the experimental weight loss of 22.9% observed at around 970 K in the TG curve over the temperature range of 850–1200 K. The experimental and theoretical weight losses, and the molecular gases eliminated by the evaporation with various temperature ranges are summarized in Table 6.

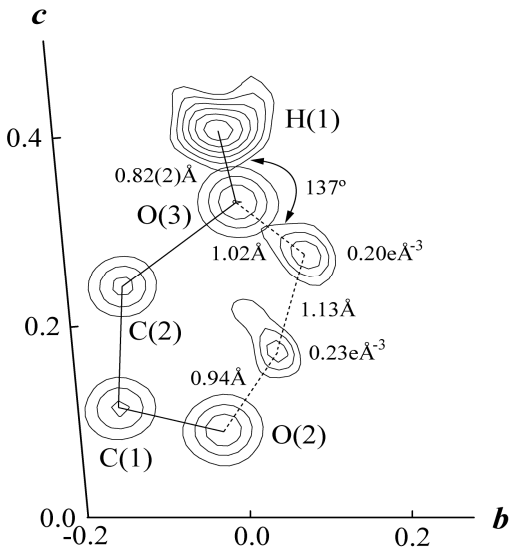

Fig. 4. Difference electron density Fourier map in the vicinity of the O(2) and O(3) atoms along the *a*-axis, containing Fourier peaks corresponding to the O(2), O(3), C(1), and C(2) atoms and a difference Fourier peak corresponding to the H(1) atom. An angle of 137° is formed between the O(3)–H(1) bond and the difference density peak of 0.20 eÅ^{-3}. The solid and short dashed lines show the separations between the density peaks

Table 4. Hydrogen-bond geometry (in Å and degrees)

D–H···A	D–H	H···A	D···A	<D–H···A
O(3)–H(1)···O(5)$^{(1)}$	0.82(2)	1.97(2)	2.7888(9)	173(1)
O(4)–H(2)···O(2)$^{(2)}$	0.82(2)	1.87(2)	2.6823(9)	178(2)
C(2)–H(3)	0.92(1)			
C(3)–H(4)	0.99(1)			
O(7)–H(5)···O(6)	0.84(2)	1.90(2)	2.731(1)	174(2)
O(7)–H(6)···O(10)$^{(3)}$	0.81(2)	2.15(2)	2.938(1)	164(2)
O(8)–H(7)···O(1)$^{(4)}$	0.79(2)	2.20(2)	2.951(1)	160(2)
O(8)–H(8)···O(1)$^{(5)}$	0.81(2)	2.05(2)	2.850(1)	173(2)
O(9)–H(9)···O(7)$^{(4)}$	0.85(2)	1.91(2)	2.755(1)	171(2)
O(9)–H(10)···O(5)$^{(6)}$	0.79(2)	2.51(2)	3.205(1)	148(2)
O(9)–H(10)···O(6)$^{(6)}$	0.79(2)	2.21(2)	2.937(1)	154(2)
O(10)–H(11)···O(6)$^{(4)}$	0.80(2)	1.95(2)	2.736(1)	167(2)
O(10)–H(12)···O(1)$^{(7)}$	0.83(2)	1.99(2)	2.802(1)	167(2)

(Symmetry codes: (1) –x,–y,–z+1; (2) –x+1,–y,–z+2; (3) x–1,y,z; (4) –x+1,–y+1,–z+1; (5) x–1,y,z–1; (6) x+1,y,z; (7) x,y,z–1.)

Table 5. Peak temperatures (including a shoulder peak temperature), transition enthalpies *ΔH*, and transition entropies *ΔS* obtained from DSC, DTA and DTG curves

DSC	Peak temp. (K)	312.2	387.8						
	ΔH (kJ mol^{-1})	2.73	136.6						
	ΔS/*R*	1.05	42.37						
DTA	Peak temp. (K)		392.3	556.0	575.9		749.1	767.1	968.2
DTG	Peak temp. (K)		390.5	562.6	575.6	724.7	747.7		964.4

(Gas constant R = 8.314 JK^{-1}mol^{-1})

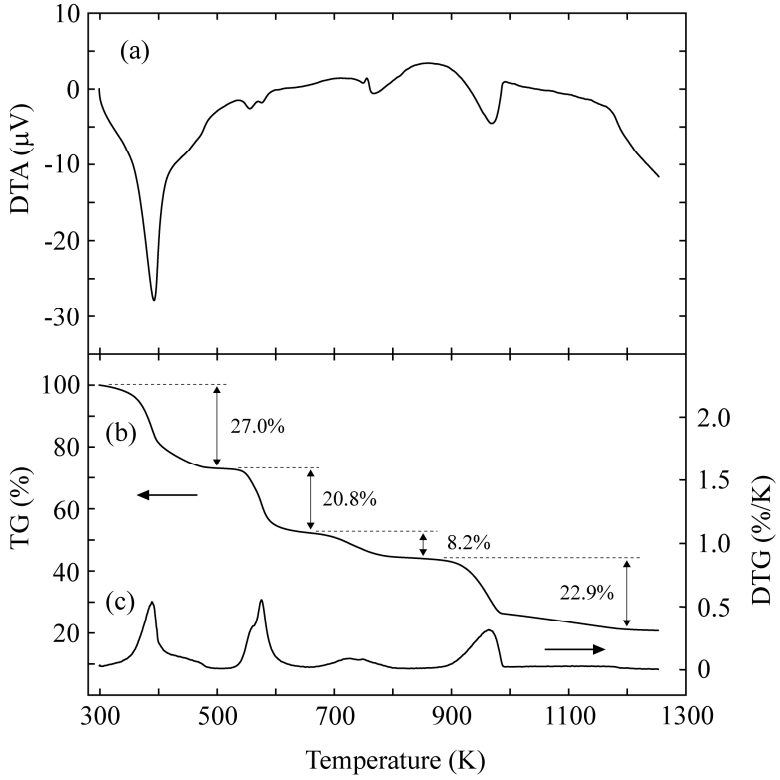

Fig. 5. DTA (a), TG (b), and DTG (c) curves of DL-$CaC_4H_4O_6 \cdot 4H_2O$ crystal on heating. Sample weight (powder) was 4.18 mg and the heating rate was 10 K min^{-1} under N_2 gas flow of 300 ml min^{-1}

Table 6. TG results of thermal decomposition process on DL-$CaC_4H_4O_6 \cdot 4H_2O$

Temp. range [K]	Weight loss (obs.) [%]	Weight loss (cal.) [%]	Elimination molecules
300–500	27.0	27.7	$4H_2O$
500–660	20.8	23.1	$2H_2CO$
660–850	8.2	6.1	$(1/2)O_2$
850–1200	22.9	21.5	2CO
Total	78.9	78.4	

The total theoretical weight loss calculated for DL-$CaC_4H_4O_6 \cdot 4H_2O$ is 78.4%. This value is very close to the total experimental weight loss of 78.9%. Thus, the slight differences between the experimental and theoretical weight loss values at each temperature range in Table 6 are probably due to the overlapping of the temperature ranges corresponding to the decomposition reactions. Summarizing the results of thermal measurements, the chemical reactions involved in the thermal decomposition of DL-$CaC_4H_4O_6 \cdot 4H_2O$ can be described by the following chemical equations:

$$CaC_4H_4O_6 \cdot 4H_2O \rightarrow CaC_4H_4O_6 + 4H_2O$$
$$CaC_4H_4O_6 \rightarrow CaC_2O_4 + 2H_2CO$$
$$CaC_2O_4 \rightarrow CaC_2O_3 + (1/2)O_2$$
$$CaC_2O_3 \rightarrow CaO + 2CO.$$

The thermal decomposition character of DL-$CaC_4H_4O_6 \cdot 4H_2O$ is very similar to that of $SrC_4H_4O_6 \cdot 4H_2O$, except for the evaporation of bound water molecules [14].

After heating the samples up to 750 or 1250 K for the measurements, black or chalky white substances were found in the open vessels, respectively. The white substance is calcium oxide, CaO, as suggested by the chemical equations described above. The chemical reaction depicted by the last term in the equations does not take place at temperatures

below 750 K, as shown in Table 6. Therefore, the black substance left in the vessel suggests the existence of carbon atoms in the sample heated to 750 K. Thus, these results for the samples heated to 750 and 1250 K support the chemical reactions highlighted above.

4. CONCLUSION

Single crystals of racemic calcium tartrate tetrahydrate, DL-$CaC_4H_4O_6{\cdot}4H_2O$, have been grown in silica gel medium by gel technique at 308 K. The thermal properties and crystal structure of the single crystals are studied by DSC, TG-DTA, and X-ray diffraction. The crystal structure at room temperature is determined to be triclinic with space group $P\bar{1}$ by means of single-crystal X-ray diffraction, and found to consist of CaO_8 dodecahedra, $C_4H_4O_6$ molecules, and hydrogen-bonding networks between adjacent $C_4H_4O_6$ molecules along the *c*-axis and between $C_4H_4O_6$ and H_2O molecules along the $[0\bar{1}1]$ direction. A phase transition is also found to occur at around 310 K from the DSC measurements. We suggest that this transition is driven by intramolecular proton transfer between the three possible positions in the vicinity of the O atoms. Weight losses during the thermal decomposition of the DL-$CaC_4H_4O_6{\cdot}4H_2O$ crystal occur in the temperature range of 300–1200 K. The chemical equations illustrating the decomposition reactions of DL-$CaC_4H_4O_6{\cdot}4H_2O$ are presented for the corresponding temperature ranges. The thermal decomposition behavior is very similar to that of $SrC_4H_4O_6{\cdot}4H_2O$, except for that related to evaporation loss of bound water molecules. It is suggested that the weight losses are caused by the evaporation of bound water molecules and the evolution of $2H_2CO$, $(1/2)O_2$, and 2CO gases, and the resulting chalky white substance in the open vessel after decomposition is calcium oxide.

COMPETING INTERESTS

Authors have declared that no competing interests exist.

REFERENCES

1. Stern F, Beevers CA. The crystal structure of tartaric acid. Acta Crystallogr. 1950;3(5): 341–346.
2. Parry GS. The crystal structure of hydrate racemic acid. Acta Crystallogr. 1951;4(2): 131–138.
3. Okaya Y, Stemple NR, Kay MI. Refinement of the structure of D-tartaric acid by X-ray and neutron diffraction. Acta Crystallogr. 1966;21(2):237–243.
4. Bootsma GA, Schoone JC. Crystal structures of mesotartaric acid. Acta Crystallogr. 1967;22(4):522–532.
5. Nie JJ, Xu DJ, Wu JY, Chiang MY. Redetermination of racemic tartaric acid monohydrate. Acta Crystallogr. 2001; E57(5):o428–o429.
6. Song QB, Teng MY, Dong Y, Ma CA, Sun J. (2S,3S)-2,3-Dihydroxy-succinic acid monohydrate. Acta Crystallogr. 2006; E62(8):o3378–o3379.
7. Derewenda ZS. On wine, chirality and crystallography. Acta Crystallogr. 2008; A64(1):246–258.
8. Fukami T, Tahara S, Yasuda C, Nakasone K. Structural refinements and thermal properties of L(+)-tartaric, D(–)-tartaric, and monohydrate racemic tartaric acid. Inter J Chem. 2016;8(2):9–21.
9. Lowry TM. Pasteur as chemist. Proc Roy Soc Med. 1923;16:16–20.
10. Desai CC, Patel AH. Crystal data for ferroelectric $RbHC_4H_4O_6$ and $NH_4HC_4H_4O_6$ crystals. J Mater Sci Lett. 1988;7(4): 371–373.
11. Abdel-Kader MM, El-Kabbany F, Taha S, Abosehly AM, Tahoon KK, El-Sharkawy AA. Thermal and electrical properties of ammonium tartrate. J Phys Chem Solids. 1991;52(5):655–658.
12. Torres ME, Peraza J, Yanes AC, López T, Stockel J, López DM, Solans X, Bocanegra E, Silgo GG. Electrical conductivity of doped and undoped calcium tartrate. J Phys Chem Solids. 2002;63(4):695–698.
13. Firdous A, Quasim I, Ahmad MM, Kotru PN. Dielectric and thermal studies on gel grown strontium tartrate pentahydrate crystals. Mull Mater Sci. 2010;33(4); 377–382.
14. Fukami T, Tahara S, Yasuda C, Nakasone K. Crystal structure and thermal properties of $SrC_4H_4O_6{\cdot}4H_2O$ single crystals. Int Res J Pure Appl Chem. 2016;11(1):1–10.
15. Hawthorne FC, Borys I, Ferguson RB. Structure of calcium tartrate tetrahydrate. Acta Crystallogr. 1982;B38(9):2461–2463.
16. Boese R, Heinemann O. Crystal structure of calcium tartrate tetrahydrate, $C_4H_4O_6Ca(H_2O)_4$. Z Kristallogr. 1993; 205(1–2):348–349.

17. Buschmann J, Luger P. Structure of potassium hydrogen (+)-tartrate at 100 K, $K^+.C_4H_5O_6^-$. Acta Crystallogr. 1985;C41(2): 206–208.
18. Pasteur ML. Sur les relations qui peuvent existre la forme cristalline, la composition chimique et le sens de la polarisation rotatoire. Ann Chim Phys. 1848;24: 442–463.
19. Tobe Y. The reexamination of Pasteur's experiment in Japan. Mendeleev Commun. 2003;13(3):93–94.
20. Gal J. The discovery of biological enantioselectivity: Louis Pasteur and the fermentation of tartaric acid, 1857 – a review and analysis 150 yr later. Chirality. 2008;20(1):5–19.
21. Gal J. Citation for chemical breakthrough awards: Choosing Pasteur's award-winning publication. Bull Hist Chem. 2013;38(1): 7–12.
22. Bail AL, Bazin D, Daudon M, Brochot A, Robbez-Massond V, Maisonneuvea V. Racemic calcium tartrate tetrahydrate [form (II)] in rat urinary stones. Acta Crystallogr. 2009;B65(3):350–354.
23. Burla MC, Caliandro R, Camalli M, Carrozzini B, Cascarano GL, Giacovazzo C, Mallamo M, Mazzone A, Polidori G, Spagna R. SIR2011: A new package for crystal structure determination and refinement. J Appl Crystallogr. 2012;45(2): 357–361.
24. Sheldrick GM. Crystal structure refinement with SHELXL. Acta Crystallogr. 2015; C71(1):3–8.
25. Farrugia LJ. WinGX and ORTEP for Windows: An update. J Appl Crystallogr. 2012;45(4):849–854.

Peer-review history:
The peer review history for this paper can be accessed here:
http://sciencedomain.org/review-history/16006